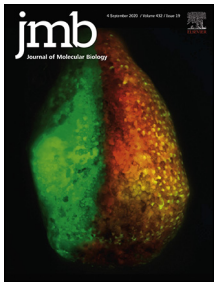

Crystal Structures of Ternary Complexes of MEF2 and NKX2–5 Bound to DNA Reveal a Disease Related Protein–Protein Interaction Interface

Xiao Lei [1 †], Jun Zhao [4], Jared M. Sagendorf [5], Niroop Rajashekar [1], Jiang Xu [1], Ana Carolina Dantas Machado [5, ‡], Chandani Sen [1, §], Remo Rohs [2, 3, 5], Pinghui Feng [4] and Lin Chen [1, 2, 3]

1 - Molecular and Computational Biology, *Department of Biological Sciences, University of Southern California, Los Angeles, CA 90089, USA*
2 - Department of Chemistry, *University of Southern California, Los Angeles, CA 90089, USA*
3 - USC Norris Comprehensive Cancer Center, *Keck School of Medicine, University of Southern California, Los Angeles, CA 90089, USA*
4 - Section of Infection and Immunity, *Herman Ostrow School of Dentistry, Norris Comprehensive Cancer Center, University of Southern California, 925 W 34th Street, Los Angeles, CA 90089, USA*
5 - Quantitative and Computational Biology, *Departments of Biological Sciences, Physics & Astronomy, and Computer Science, University of Southern California, Los Angeles, CA 90089, USA*

Correspondence to Xiao Lei and Lin Chen: *Molecular and Computational Biology, Department of Biological Sciences, University of Southern California, Los Angeles, CA 90089, USA. xiaoleiusc@gmail.com, linchen@usc.edu*
https://doi.org/10.1016/j.jmb.2020.07.004
Edited by Dylan Taatjes

Abstract

MEF2 and NKX2–5 transcription factors interact with each other in cardiogenesis and are necessary for normal heart formation. Despite evidence suggesting that these two transcription factors function synergistically and possibly through direct physical interactions, molecular mechanisms by which they interact are not clear. Here we determined the crystal structures of ternary complexes of MEF2 and NKX2–5 bound to myocardin enhancer DNA in two crystal forms. These crystal structures are the first example of human MADS-box/homeobox ternary complex structures involved in cardiogenesis. Our structures reveal two possible modes of interactions between MEF2 and NKX2–5: MEF2 and NKX bind to adjacent DNA sites to recognize DNA in cis; and MEF2 and NKX bind to different DNA strands to interact with each other in trans *via* a conserved protein–protein interface observed in both crystal forms. Disease-related mutations are mapped to the observed protein–protein interface. Our structural studies provide a starting point to understand and further study the molecular mechanisms of the interactions between MEF2 and NKX2.5 and their roles in cardiogenesis.

Introduction

The MADS-box family transcription factor myocyte-enhancer factor 2 (MEF2) and the homeobox family transcription factor NKX2–5 play important roles in cardiogenesis [1–4] and have also been implicated in carcinogenesis [5–11]. Deletion of MEF2 or NKX2–5 causes embryonic death in mice with defects in heart development [12–14]. Mutations or misexpressions of MEF2 and NKX2–5 are frequently found in congenital heart disease and leukemia/lymphoma patients [10,15–24].

The functional synergy between MEF2 and NKX2–5 in cardiogenesis has long been postulated [25,26] based on experimental observations that MEF2 and NKX2–5 expression coincides with each other in cardiac muscle development, and the studies that suggest MADS-box protein and homeobox protein could interact with each other [27,28]. Co-immunoprecipitation and mammalian two-hybrid assays detected physical interactions between MEF2 and NKX2–5 in cells [29]. Chip-Seq studies show that MEF2 and NKX2–5 co-occupy active cardiac enhancer regions with other transcription factors such

as GATA-4, TBX5 and SRF to initiate cardiac differentiation and maintain cardiac gene expression [30–33]. Furthermore, MEF2 and NKX2–5 have been shown as important factors in the reprogramming of fibroblasts into cardiomyocytes [34–38]. To further understand the molecular interactions between MEF2 and NKX2–5, we determined the co-crystal structures of ternary complexes of MEF2 and NKX2–5 bound to myocardin enhancer DNA in two crystal forms. Our structures reveal new insights into the interaction mechanisms between these two important transcription factors that are involved in the heart development.

Results and Discussion

The overall structure of the MEF2/NKX2–5/DNA complex

Before crystallography studies, we did electrophoretic mobility shift assays (EMSA) to study the ability of MEF2, NKX2–5 and DNA to form ternary complexes. The DNA in our EMSA and crystallization studies is designed based on the composite regulatory elements that regulate myocardin expression. Myocardin is a common transcriptional downstream target of MEF2 and NKX2–5 [31,39–41]. We analyzed Chip-seq peaks of MEF2 and NKX2–5 from literature in public Chip-seq databases [42], and found that many MEF2 and NKX2–5 binding sites were in the myocardin gene regulatory regions (Supplemental Figure 1). We chose one composite regulatory element that contains adjacent MEF2 and NKX2–5 sites from myocardin enhancer (MyE) in our EMSA assays and crystallization studies. The EMSA results indicate that MEF2, NKX2–5 and myocardin enhancer DNA form stable ternary complexes (Figure 1(a)). We used MEF2 and NKX2–5 protein constructs that contain the MEF2 MADS-box and MEF2-specific domain (residues 1–95) and the NKX2–5 homeobox domain (residues 137–197) (Supplemental Figure 2) in the crystallization of MEF2/NXK2–5/DNA ternary complexes. We determined the MEF2/NKX2–5/DNA structures in two crystal forms, each from different MEF2 constructs: MEF2 Chimera/NKX2–5/DNA ternary complex at 2.1 Å resolution and MEF2B/NKX2–5/DNA at 2.9 Å resolution (Table 1). MEF2 Chimera is a MEF2 construct with the MADS-box domain from MEF2A and the MEF2-specific domain from MEF2B. MEF2 Chimera has over 90 % amino acids identity as other MEF2 members (MEF2A-MEF2D) (Supplemental Figure 2a), and is biochemically characterized as similar to wild-type MEF2 in previous studies [43]. The purpose of using MEF2 Chimera construct is to increase the chance of successful crystallization and

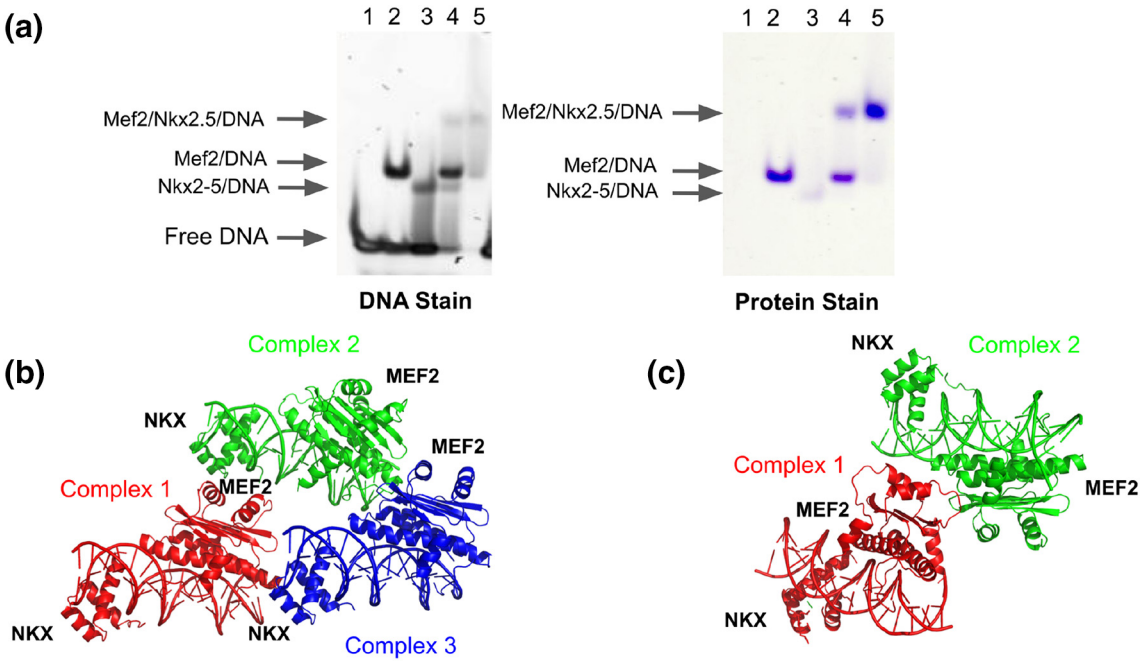

Figure 1. MEF2 and NKX2–5 form ternary complexes on DNA. (a) EMSA of MEF2, NKX2–5 binding to myocardin enhancer DNA element (MyE). The MyE DNA sequence, 5′-CACTATTTTAAGAAAGTGCTT-3′, contains adjacent MEF2 and NKX2–5 binding sites. The molar ratios of DNA, MEF2, and NKX2–5 are 1: 1: 1 in lane 4 and 1: 1: 2 in lane 5 (see the Materials and Methods section for details). (b) Overall crystal structure of the MEF2 Chimera/NKX2–5/DNA ternary complex. Three sets of complexes in asymmetric units are colored in red, green and blue, respectively. (c) Overall crystal structure of the MEF2B/NKX2–5/DNA ternary complexes. Two sets of complexes in asymmetric units are colored in red and green, respectively.

Table 1. Data collection and refinement statistics

	MEF2BWT/NKX2–5/DNA	MEF2ChimWT/NKX2–5/DNA
Resolution range	47.46–2.90 (3.00–2.90)	49.28–2.10 (2.18–2.10)
Space group	*P* 21 21 21	*P* 21 21 21
Cell dimensions		
a, *b*, *c* (Å)	66.04, 93.24, 136.5	69.37, 133.91, 40.04
α, β, γ (°)	90, 90, 90	90, 90, 90
Total reflections	74,630 (7279)	499,421 (47,928)
Unique reflections	18,336 (1904)	76,673 (7471)
Multiplicity	4.1 (3.8)	6.5 (6.4)
Completeness (%)	94.3 (99.6)	99.7 (98.9)
Mean *I*/sigma(*I*)	11.3 (3.0)	12.9 (3.0)
Wilson *B*-factor	60.64	35.73
R-merge	0.079 (0.580)	0.077 (0.608)
R-meas	0.089 (0.665)	0.084 (0.661)
R-pim	0.042 (0.319)	0.033 (0.257)
CC1/2	0.997 (0.815)	0.997 (0.854)
CC[a]	0.999 (0.948)	0.999 (0.960)
Reflections used in refinement	18,220 (1901)	76,582 (7468)
Reflections used for *R*-free	878 (93)	3802 (350)
R-work	0.206 (0.320)	0.188 (0.264)
R-free	0.254 (0.357)	0.225 (0.290)
CC (work)	0.954 (0.845)	0.965 (0.842)
CC (free)	0.932 (0.778)	0.968 (0.811)
Number of non-hydrogen atoms	5706	8973
Macromolecules	5703	8528
Solvent	3	445
Protein residues	469	704
RMS (bonds)	0.012	0.015
RMS (angles)	1.55	2.05
Average *B*-factor	70.4	47.85
Macromolecules	70.42	48.16
Solvent	23.72	42.01

[a] Values in parentheses are for the highest-resolution shell.

better resolution. There are three sets of ternary complexes in the asymmetric unit of the MEF2 Chimera/NKX2–5/DNA crystal structure and two sets of ternary complexes in the asymmetric unit of the MEF2B/NKX2–5/DNA crystal structure (Figure 1 (b) and (c)). The overall folds of MEF2 and NKX2–5 are identical within the multiple copies in the asymmetric unit of the two crystal forms and also identical to their respective counterparts in previously published structures (Supplemental Figure 3a, b) [44,45]. The structural features we present in this paper are conserved between the two crystal structures. Because MEF2 Chimera/NKX2–5/DNA crystals have better resolution, our structure analyses are based mainly on this structure unless indicated otherwise.

Protein–DNA interactions

MEF2 and NKX2–5 interact with DNA from opposite faces of the DNA double helix in the ternary complex. Consistent with previous literature reports, MEF2 interacts mainly with DNA minor groove through helix H1 and the N-terminal extension, and NKX2–5 interacts mainly with DNA major groove through helix H3 of the homeodomain (Figure 2(a), Supplemental Figure 4). MEF2 and NKX2–5 bind to overlapping DNA regions at the junction of their binding sites. The N-terminal extension from MEF2 and the N-terminal extension from NKX2–5 interact with the same minor groove region (Figure 2(a)). Moreover, K23 of MEF2 and R142 of NKX2–5 interact with the same AT base pair from the major and minor groove, respectively (Figure 2(b)). Interestingly, the NKX2–5 R142C mutation, which is found in congenital heart defects patients, has reduced DNA affinity and diminished synergistic interaction with transcription partner MEF2, TBX5, and GATA4 in mouse models and biochemical assays [46–49]. There is a cation pi interaction between MEF2 R15 and NKX2–5 Y191; both residues are involved in DNA interaction: MEF2 R15 interacts with DNA phosphate backbone, and NKX2–5 Y191 interacts with bases A5′ and C6′ (Figure 2(c)). MEF2 R15 and NKX2–5 Y191 residues are conserved in MEF2 family proteins and NKX family proteins respectively [45,50], and residues Y191 are reported to be an important residue involving specific interaction between NKX2–5 and NK2 element [45]. There is no obvious DNA bending in our MEF2/NKX2–5/DNA structures as compared to

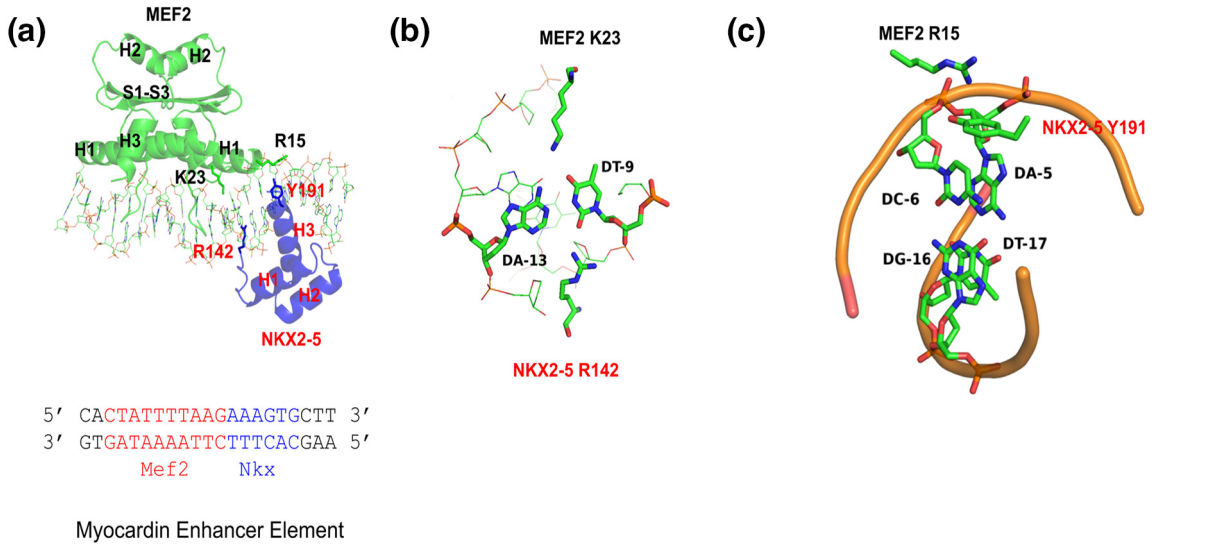

Figure 2. Protein and DNA interaction features of MEF2/NKX2–5/DNA structure. (a) MEF2 chimera/NKX2–5/DNA ternary complex structure. DNA interacting residues of interests (MEF2 R15 and K23, NKX2–5 R142 and Y191) are shown as sticks. The sequence of the DNA in the crystal is shown below, with the MEF2 binding site colored in red and the NKX2–5 binding site colored in blue. H1–H3: helix 1–3; S1-S3: beta strand 1–3. (b) MEF2 K23 and NKX2–5 R142 interact with the same AT base pair from the major and minor groove, respectively. (c) Cation ion and pi interaction between MEF2 R15 and NKX2–5 Y191. MEF2 R15 interacts with phosphate backbone of A-5′. NKX2–5 Y191 interacts with the bases of A-5′ and C-6′.

published ternary structures involving MADS-box family members such as the yeast MCM1/Matα2/DNA and the human SRF/SAP-1/DNA ternary structures (Supplemental Figure 5) [28,51,52]. There is no protein–protein interaction involving secondary structural elements between MEF2 and NKX2–5 in our crystal structures, which is in contrast to the yeast MCM1/Matα2/DNA and the human SRF/SAP-1/DNA ternary structures, in which there are direct protein–protein interactions between strand S2 of the MADS-box domain and another beta strand from co-factors (Supplemental Figure 5) [28,51,52]. As the protein constructs in our crystallization studies only contain the MADS-box and MEF2-specific domain of MEF2 and homeobox domain of NKX2–5, we could not rule out the possibility that other parts in the full length MEF2 and NKX2–5 proteins may interact with each other in this cis-mode.

Protein–protein interaction interface

In the crystal structures, we noticed a protein–protein interaction interface (with buried surface area around 359.6 Å^2) between a MEF2 dimer bound to one DNA duplex and a NKX2–5 molecule bound to another DNA duplex in symmetry related complexes. We refer to this as the trans interaction mode. This protein–protein interaction interface is conserved in both the MEF2 Chimera/NKX2–5/DNA crystal structure and the MEFB/NKX2–5/DNA crystal structure. In this interface, the MEF2-specific domain strand S3 and helix H3 interact with helix H1, loop1 and helix H2 from NKX2–5 homeobox domain (Figure 3(a)). This interface shows remarkable chemical and shape complementarity: charge–charge interactions between MEF2 E74 and NKX2–5 R155, and MEF2 R79 and NKX2–5 E167; hydrogen bonding interactions between the main chain of MEF2 H76, S78, and the side chains of NKX2–5 R156, E167, and Q170; and a cation–pi interaction between MEF2 R90 and NKX2–5 Y162 (Figure 3(b) and (c)). Residues in this protein–protein interaction interface are evolutionarily conserved (Figure 4(a)). Mutations associated with heart disease such as NKX2–5 Q160P and L171P are mapped in this interface (Figure 4(b) and (c)) [17,53–56], these disease mutations are likely disrupting MEF2 and NKX2–5 interaction. These analyses suggest that the MEF2 and NKX2–5 interaction interfaces observed in our structures are likely to be functionally important. This interface also harbors residues that have been reported to be subject to post-translational modifications in the literature; for example, MEF2 T80 and NKX2–5 and NKX2–5 S164 could be modified by phosphorylation [57–59]. Further studies are needed to test if these disease mutations and post-translational modifications impact the interaction between MEF2 and NKX2–5.

Our study indicates that the MEF2-specific domain could be an important interaction interface for cofactor interactions. This novel cofactor interaction interface is distinct from the classical MEF2 cofactor binding groove formed by the MEF2-specific domain

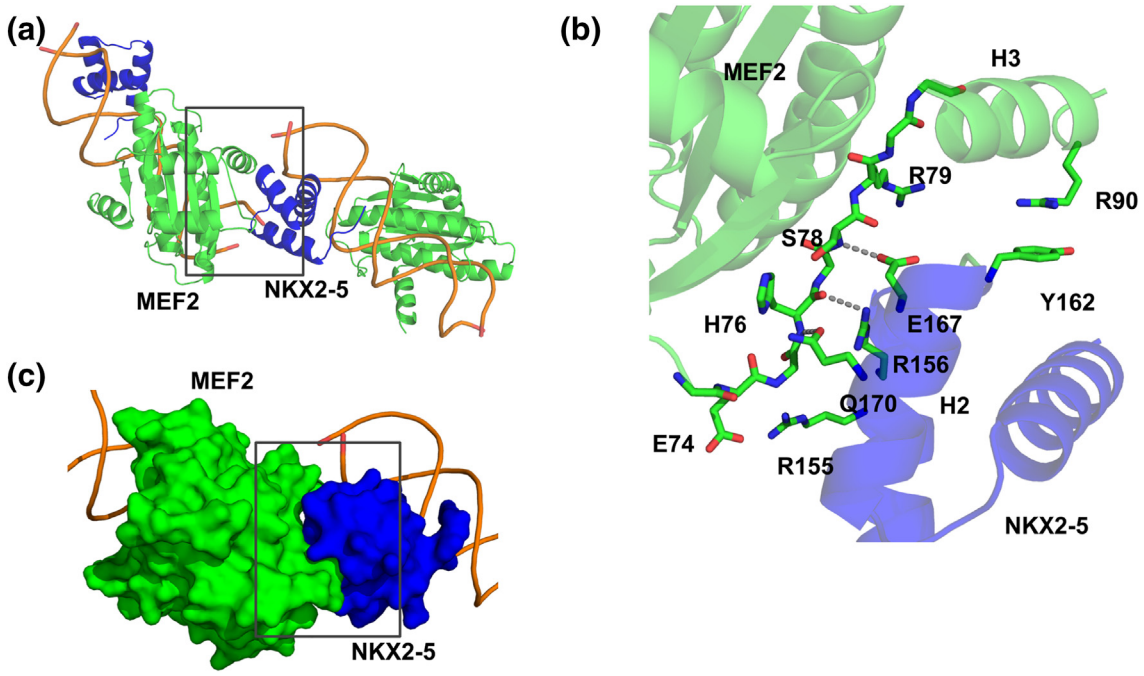

Figure 3. The conserved MEF2 and NKX2–5 protein–protein interaction interface in two crystal forms. (a) Direct protein–protein interaction interface between MEF2 and NKX2–5 from symmetry related complexes. (b) Detailed interactions of residues involved in the protein–protein interaction interface. Dashed line indicates hydrogen bonds. (c) MEF2 and NKX2–5 protein–protein interaction interface represented in surface mode. H3: MEF2 helix 3. H2: NKX2–5 helix 2.

helix H2 and strand S1–S3 [44,60,61]. Our structures could explain previous observations in the literature that MEF2C VLL65-67ASR mutants that were unable to bind histone deacetylase (HDAC4) could interact with the bHLH family member myogenin [62]. According to our model, the VLL65-67ASR mutations disrupt classical MEF2 co-factor interaction groove, which is responsible for class IIa HDAC interaction but not for myogenin interaction; myogenin interacts with MEF2 through MEF2-specific domain, as mutations (E77V/S78N/R79Q/T80A or N73I/E74A/H76L) in MEF2-specific domain disrupts MEF2 and myogenin interaction and synergistic activation of target genes [63].

However, we were unable to detect MEF2 and NKX2–5 interaction *in vitro* using two DNA oligomers with one containing a MEF2 binding site and the other containing a NKX2–5 binding site, and the MEF2 and NKX2–5 protein fragments used in our crystallography study (data not shown). One possibility is that the stable interaction by this interface requires full-length MEF2 or NKX2–5 proteins wherein other parts of MEF2 and NKX2–5 may contribute to the overall interaction stability. Another possibility is that the interaction inferred by this interface is a weak and transient interaction in solution but would be further stabilized by other proteins in cellular contexts. Our preliminary data show that the interaction of DNA with either or both MEF2C and NKX2–5 is important for their mutual interactions, as nuclease treatment disrupts the interaction between MEF2C and NKX2–5 in pull-down assays (Supplemental Figure 6).

In conclusion, our studies suggest that MEF2 and NKX2–5 could interact with each other through at least two different modes: by binding adjacent and overlapping DNA regions in cis on the same DNA strands and interactions in trans across different DNA strands through a conserved protein–protein interaction interface. The latter could also have implications for long-range chromatin interactions (e.g., enhancer–promoter interaction) mediated by transcription machinery containing MEF2 and NKX2–5 proteins. This model of long range chromatin interactions is consistent with the observations that NKX2–5 and MEF2 are found in super-enhancers [64,65]. Further functional and genome structural studies are needed to test the biological roles of this interface in cell and animal models, and the crystal structures presented in this study provide a foundation for these studies.

Materials and Methods

Protein purification

MEF2 Chimera (residues 1–95) and MEF2B (residues 1–93), which contain MADS-box domain (residues 1–57) and MEF2-specific domain (residues

(a)

Human	MEF2A	75-PHESRTNSDIVEALNK-90	Human	NKX2.5	155-RRFKQQRYLSA-165
Human	MEF2B	75-PHESRTNTDILETLKR-90	Human	NKX2.1	178-RRFKQQKYLSA-188
Human	MEF2C	75-PHESRTNSDIVETLRK-90	Human	NKX2.3	165-RRFKQQRYLSA-175
Mouse	MEF2C	75-PHESRTNSDIVETLRK-90	Mouse	NKX2.5	155-RRFKQQRYLSA-165
Rat	MEF2C	75-PHESRTNSDIVETLRK-90	Rat	NKX2.5	155-RRFKQQRYLSA-165
Chicken	MEF2C	75-PHESRTNSDIVETLRK-90	Chicken	NKX2.5	155-RRFKQQKYLSA-165
Zebrafish	MEF2C	75-PHESRTNSDIVETLRK-90	Zebrafish	NKX2.5	155-RRFKQQKYLSA-165

(b)

NKX2-5 mutations	Disease
Q160P	ASD, AVB
R161P	TD
E167fs	ASD,VSD,AVB
L171P	ASD,VSD,AVB

(c)

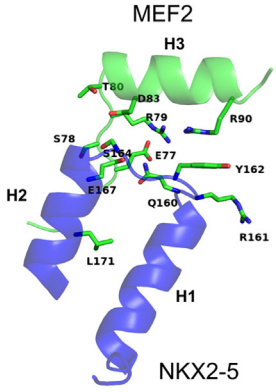

Figure 4. MEF2 and NKX2–5 protein–protein interaction interface is evolutionary conserved. (a) Sequence alignment of MEF2 and NKX2–5 interface across species. Identical amino acids are colored in red. Amino acids with strong similar properties are colored in blue. (b) NKX2–5 disease related mutations in the interface region in literature. ASD, atrial septal defect; AVB: atrioventricular block; VSD, ventricular septal defect; TD: thyroid dysgenesis. fs: frameshift mutation. (c) Disease-relevant residues of NKX2–5 are shown as sticks in the MEF2 and NKX2–5 interaction interface. Residues from MEF2 that are involving interactions with these NKX2–5 residues are shown as sticks and labeled in green. Although NKX2–5 L171 is not involved in direct contact with MEF2, the L171P mutation may impact NKX2–5 and MEF2 interaction as proline is considered to be an alpha helix breaker.

58–95) were purified as previously described [43]. The final storage buffer for MEF2B WT, MEF2 Chimera was as follows: 10 mM Hepes (pH 7.5), 200 mM NaCl, 0.5 mM EDTA, and 0.5 mM TCEP.

NKX2–5 homeobox domain (residues 138–197) with C193S was cloned into pET28 vector for crystallization [45]. The protein was expressed as sumo fusion protein with both 6× His-tag and sumo tag at its N terminus in *Escherichia coli* BL21(DE3) pLysS cells. Protein expression was induced in 1 L 2XYT medium with 0.5 mM IPTG at 22 °C overnight (16 to 20 h). Protein was initially purified by QIAGEN Ni-NTA agarose. The His-tag and sumo-tag were cleaved by Ulp-1 enzyme, and the protein was further purified by heparin Fastflow column (GE Healthcare) with buffer A containing 20 mM Hepes (pH 7.0), 0.5 mM EDTA, and 0.5 mM TCEP and buffer B containing all the components in buffer A and 1.5 M NaCl. Protein peak fractions were pooled together and subject to final Superdex 75 (GE Healthcare) size exclusion column purification with buffer as follows: 10 mM Hepes (pH 7.5), 200 mM NaCl, and 0.5 mM TCEP.

DNA purification

The DNA used in crystallization for MEF2 Chimera/NKX2–5/DNA ternary complex is 5′ CACTATTTTAA GAAAGTGCTT 3′ and its complementary strand 5′ AAGCACTTTCTTAAAATAGTG 3′. The DNA used in crystallization for MEF2B/NKX2–5/DNA is 5′ CCACTATTTTAAGAAAGTGCTT 3′ and its complementary strand 5′ AAGCACTTTCTTAAAATAGTGG 3′. DNA was purchased from Integrated DNA Technologies (Coralville, IA) at 1-μmol scale in the crude and desalted form. The crude DNA was dissolved in a 10 mM NaOH and purified by a Mono Q cation-exchange column (GE Healthcare) on FPLC (GE Healthcare) as previously described [66]. Complementary DNA strands were annealed at 95 °C in the annealing buffer (100 mM NaCl, 5 mM Hepes (pH 7.6)) in PCR machine (Eppendorf Mastercycler Personal 5332 Thermal Cycler) for 2 min and cool to room temperature on bench for 1 h.

EMSA

EMSA was performed in 20 mM Hepes (pH 7.6), 250 mM NaCl, 1 mM DTT, 12% glycerol in a 10 μl volume. The final concentration of DNA was kept at 10 μM. The final concentration of MEF2 Chim WT (residues 1–95) and MEF2B (residues 1–93) was kept at 10 μM. The final NKX2–5 (residues 138–197) concentration was kept at 10 μM (DNA: MEF2: NKX2–5 molar ratio 1:1:1) or 20 μM (DNA: MEF2: NKX2–5 molar ratio 1:1:2). The binding reactions

were analyzed on a 4%–20% (w/v) acrylamide gradient native gel in TBE and stained with Sybr Safe DNA Dye (Thermo Fisher Scientific).

Crystallization and structure determination

MEF2, NKX2–5, and DNA were mixed at a molar ratio of 1:1:1.2, and the final protein concentration in the mixture was around 10 to 15 mg/ml. Sitting drop crystal trays were set up by a crystallization robot (Crystal Gryphon from Art Robbins Instruments) at 18 °C, in which 0.4 μl protein complex and 0.4 μl mother liquor were mixed. MEF2 Chimera/NKX2–5/DNA crystals appeared within 3 weeks with rod shape in crystallization buffer (0.15 M DL-Malic acid (pH 7.0), 20% polyethylene glycol (PEG) 3350). Crystals were harvested, cryoprotected in the crystallization buffer with increased PEG concentration to 35%, and flash frozen in liquid nitrogen. MEF2B/NKX2–5/DNA crystals appeared within 3 weeks with needle or plate shape in crystallization buffer (100 mM Hepes (pH 7.0), 18% PEG 2000). Crystals were harvested and cryoprotected in the crystallization buffer with 30% PEG 400 as cryoprotectant. Data were collected at Advanced Photon Source (APS Chicago) beamline 23 ID-B. Crystal diffraction data were processed with iMosflm and initial space group assignment by pointless in CCP4 suite [67–69]. The MEF2 Chimera/NKX2–5/DNA and MEF2B/NKX2–5/DNA ternary complex structures were determined by molecular replacement with Phaser in CCP4 suite using MEF2/DNA complex (PDB: 1N6J) and NKX2–5/DNA complex (PDB: 3RKQ) as partial search models [44,45,70]. Model building was done in Coot, and refinement was done in Refmac5, Phenix refine, and PDB_REDO [71–75]. Composite omit maps were generated by "Composite omit map" tool in Phenix suite [76–78]. Crystallographic and refinement statistics table (Table 1) was generated by utility tools in Phenix suite [72].

Protein sequence alignment was performed with the Clustal Omega [79] and visualized with ESPript 3.0 [80], and protein and DNA interaction plots are generated with the DNAproDB tool [81].

Chip-seq data analysis

MEF2C and NKX2–5 Chip-seq data were retrieved from ChIP-Atlas database [42] and visualized in IGV browser [82].

Co-immunoprecipitation and immunoblotting

HEK293T cells were transfected with the indicated expression plasmids for 48 h. Whole-cell lysates were prepared with NP40 buffer (50 mM Tris–HCl (pH 7.4), 150 mM NaCl, 1% NP-40, 5 mM EDTA) supplemented with 20 mM β-glycerophosphate and 1 mM sodium orthovanadate. Whole-cell lysates were sonicated, centrifuged, and pre-cleared with protein A/G agarose for 1 h. Pre-cleared samples were then incubated with the indicated antibody-conjugated agarose overnight at 4 °C. The agarose beads were washed extensively, and samples were eluted by boiling at 95 °C for 10 min. Precipitated proteins were analyzed by SDS gel electrophoresis and immunoblotting.

Immunoblotting was performed using the indicated primary antibodies (1:1000 dilution) and IRDye800-conjugated secondary antibodies (1:10,000 dilution, LI-COR). Proteins were visualized by Odyssey infrared imaging system (LI-COR).

Data availability

Coordinates and structure factors have been deposited in the PDB with accession numbers 6WC2 (MEF2 Chimera/NKX2–5/DNA complex) and 6WC5 (MEF2B/NKX2–5/DNA complex).

Acknowledgments

The work was supported by the National Institutes of Health (R01AI113009, 5U54DK107981, and R21HG010528 to L.C. and R35GM130376 to R.R.).

Appendix A. Supplementary data

Supplementary data to this article can be found online at https://doi.org/10.1016/j.jmb.2020.07.004.

Received 20 May 2020;
Received in revised form 8 July 2020;
Accepted 9 July 2020
Available online 15 July 2020

Keywords:
MEF2;
NKX2–5;
transcription regulation;
protein–protein interaction;
cardiogenesis

Present address: X. Lei, The Rockefeller University.
Present address: A.C. Dantas Machado, University of California, San Diego.
Present address: C. Sen, University of California, Los Angeles.

Abbreviations used:
MEF2, myocyte-enhancer factor 2; EMSA, electrophoretic mobility shift assay.

References

1. Lints, T.J., Parsons, L.M., Hartley, L., Lyons, I., Harvey, R.P., (1993). Nkx-2.5: a novel murine homeobox gene expressed in early heart progenitor cells and their myogenic descendants. *Development*, **119**, 419–431.
2. Duprey, P., Lesens, C., (1994). Control of skeletal muscle-specific transcription: involvement of paired homeodomain and MADS domain transcription factors. *Int. J. Dev. Biol.*, **38**, 591–604.
3. Shore, P., Sharrocks, A.D., (1995). The MADS-box family of transcription factors. *Eur. J. Biochem.*, **229**, 1–13.
4. Potthoff, M.J., Olson, E.N., (2007). MEF2: a central regulator of diverse developmental programs. *Development*, **134**, 4131–4140.
5. S. Nagel, M. Kaufmann, H.G. Drexler, R.A.F. MacLeod, The cardiac homeobox gene NKX2–5 is deregulated by juxtaposition with BCL11B in pediatric T-ALL cell lines via a novel t(5;14)(q35.1;q32.2), Cancer Res. 63 (2003) 5329–5334.
6. Nagel, S., Meyer, C., Quentmeier, H., Kaufmann, M., Drexler, H.G., MacLeod, R.A.F., (2008). MEF2C is activated by multiple mechanisms in a subset of T-acute lymphoblastic leukemia cell lines. *Leukemia*, **22**, 600–607.

[7] Su, X., Della-Valle, V., Delabesse, E., Azgui, Z., Berger, R., Merle-Béral, H., Bernard, O.A., Nguyen-Khac, F., (2008). Transcriptional activation of the cardiac homeobox gene CSX1/NKX2–5 in a B-cell chronic lymphoproliferative disorder. *Haematologica*, **93**, 1081–1085.

8. Morin, R.D., Mendez-Lago, M., Mungall, A.J., Goya, R., Mungall, K.L., Corbett, R.D., Johnson, N.A., Severson, T.M., et al., (2011). Frequent mutation of histone-modifying genes in non-Hodgkin lymphoma. *Nature*, **476**, 298–303.

[9] Homminga, I., Pieters, R., Langerak, A.W., de Rooi, J.J., Stubbs, A., Verstegen, M., Vuerhard, M., Buijs-Gladdines, J., et al., (2011). Integrated transcript and genome analyses reveal NKX2-1 and MEF2C as potential oncogenes in T cell acute lymphoblastic leukemia. *Cancer Cell*, **19**, 484–497.

10. Pon, J.R., Marra, M.A., (2016). MEF2 transcription factors: developmental regulators and emerging cancer genes. *Oncotarget*, **7**, 2297–2312.
11. Brescia, P., Schneider, C., Holmes, A.B., Shen, Q., Hussein, S., Pasqualucci, L., Basso, K., Dalla-Favera, R., (2018). MEF2B instructs germinal center development and acts as an oncogene in B cell lymphomagenesis. *Cancer Cell*, **34**, 453–465.e9.
12. Lin, Q., Schwarz, J., Bucana, C., Olson, E.N., (1997). Control of mouse cardiac morphogenesis and myogenesis by transcription factor MEF2C. *Science*, **276**, 1404–1407.

[13] Lyons, I., Parsons, L.M., Hartley, L., Li, R., Andrews, J.E., Robb, L., Harvey, R.P., (1995). Myogenic and morphogenetic defects in the heart tubes of murine embryos lacking the homeo box gene Nkx2–5. *Genes Dev.*, **9**, 1654–1666.

14. Tanaka, M., Chen, Z., Bartunkova, S., Yamasaki, N., Izumo, S., (1999). The cardiac homeobox gene Csx/Nkx2.5 lies genetically upstream of multiple genes essential for heart development. *Development.*, **126**, 1269–1280.
15. Bruneau, B.G., (2002). Transcriptional regulation of vertebrate cardiac morphogenesis. *Circ. Res.*, **90**, 509–519.
16. Bruneau, B.G., (2013). Signaling and transcriptional networks in heart development and regeneration. *Cold Spring Harb. Perspect. Biol.*, **5**, a008292.

[17] Schott, J.-J., Woodrow Benson, D., Basson, C.T., Pease, W., Michael Silberbach, G., Moak, J.P., Maron, B.J., Seidman, C.E., et al., (1998). Congenital heart disease caused by mutations in the transcription factor NKX2–5. *Science*, **281**, 108–111.

[18] Chung, I.-M., Rajakumar, G., (2016). Genetics of congenital heart defects: the NKX2–5 gene, a key player. *Genes*, **7**, https://doi.org/10.3390/genes7020006.

[19] Reamon-Buettner, S.M., Hecker, H., Spanel-Borowski, K., Craatz, S., Kuenzel, E., Borlak, J., (2004). Novel NKX2–5 mutations in diseased heart tissues of patients with cardiac malformations. *Am. J. Pathol.*, **164**, 2117–2125.

20. Wamstad, J.A., Alexander, J.M., Truty, R.M., Shrikumar, A., Li, F., Eilertson, K.E., Ding, H., Wylie, J.N., et al., (2012). Dynamic and coordinated epigenetic regulation of developmental transitions in the cardiac lineage. *Cell*, **151**, 206–220.
21. Qiao, X.-H., Wang, F., Zhang, X.-L., Huang, R.-T., Xue, S., Wang, J., Qiu, X.-B., Liu, X.-Y., et al., (2017). MEF2C loss-of-function mutation contributes to congenital heart defects. *Int. J. Med. Sci.*, **14**, 1143–1153.
22. Nagel, S., Venturini, L., Meyer, C., Kaufmann, M., Scherr, M., Drexler, H.G., Macleod, R.A., (2011). Transcriptional deregulation of oncogenic myocyte enhancer factor 2C in T-cell acute lymphoblastic leukemia. *Leuk. Lymphoma.*, **52**, 290–297.
23. Rajasingh, J., Bord, E., Hamada, H., Lambers, E., Qin, G., Losordo, D.W., Kishore, R., (2007). STAT3-dependent mouse embryonic stem cell differentiation into cardiomyocytes: analysis of molecular signaling and therapeutic efficacy of cardiomyocyte precommitted mES transplantation in a mouse model of myocardial infarction. *Circ. Res.*, **101**, 910–918.
24. Cante-Barrett, K., Pieters, R., Meijerink, J.P., (2014). Myocyte enhancer factor 2C in hematopoiesis and leukemia. *Oncogene*, **33**, 403–410.
25. Olson, E.N., Perry, M., Schulz, R.A., (1995). Regulation of muscle differentiation by the MEF2 family of MADS box transcription factors. *Dev. Biol.*, **172**, 2–14.
26. Molkentin, J.D., Firulli, A.B., Black, B.L., Martin, J.F., Hustad, C.M., Copeland, N., Jenkins, N., Lyons, G., et al., (1996). MEF2B is a potent transactivator expressed in early myogenic lineages. *Mol. Cell. Biol.*, **16**, 3814–3824.
27. Herskowitz, I., (1989). A regulatory hierarchy for cell specialization in yeast. *Nature*, **342**, 749–757.
28. Tan, S., Richmond, T.J., (1998). Crystal structure of the yeast MATalpha2/MCM1/DNA ternary complex. *Nature*, **391**, 660–666.
29. Vincentz, J.W., Barnes, R.M., Firulli, B.A., Conway, S.J., Firulli, A.B., (2008). Cooperative interaction of Nkx2.5 and Mef2c transcription factors during heart development. *Dev. Dyn*, **237**, 3809–3819.
30. Rojas, A., Kong, S.W., Agarwal, P., Gilliss, B., Pu, W.T., Black, B.L., (2008). GATA4 is a direct transcriptional activator of cyclin D2 and Cdk4 and is required for cardiomyocyte proliferation in anterior heart field-derived myocardium. *Mol. Cell. Biol.*, **28**, 5420–5431.

[31] He, A., Kong, S.W., Ma, Q., Pu, W.T., (2011). Co-occupancy by multiple cardiac transcription factors identifies transcriptional enhancers active in heart. *Proc. Natl. Acad. Sci.*, **108**, 5632–5637.

32. Schlesinger, J., Schueler, M., Grunert, M., Fischer, J.J., Zhang, Q., Krueger, T., Lange, M., Tönjes, M., et al., (2011). The cardiac transcription network modulated by Gata4, Mef2a, Nkx2.5, Srf, histone modifications, and microRNAs. *PLoS Genet*, **7**, e1001313.

[33] Luna-Zurita, L., Stirnimann, C.U., Glatt, S., Kaynak, B.L., Thomas, S., Baudin, F., Samee, M.A.H., He, D., et al., (2016). Complex interdependence regulates heterotypic transcription factor distribution and coordinates cardiogenesis. *Cell*, **164**, 999–1014.

[34] Sepulveda, J.L., Vlahopoulos, S., Iyer, D., Belaguli, N., Schwartz, R.J., (2002). Combinatorial expression of GATA4, Nkx2–5, and serum response factor directs early cardiac gene activity. *J. Biol. Chem.*, **277**, 25775–25782.
35. Ieda, M., Fu, J.-D., Delgado-Olguin, P., Vedantham, V., Hayashi, Y., Bruneau, B.G., Srivastava, D., (2010). Direct reprogramming of fibroblasts into functional cardiomyocytes by defined factors. *Cell.*, **142**, 375–386.
36. Addis, R.C., Ifkovits, J.L., Pinto, F., Kellam, L.D., Esteso, P., Rentschler, S., Christoforou, N., Epstein, J.A., et al., (2013). Optimization of direct fibroblast reprogramming to cardiomyocytes using calcium activity as a functional measure of success. *J. Mol. Cell. Cardiol.*, **60**, 97–106.
37. Song, K., Nam, Y.-J., Luo, X., Qi, X., Tan, W., Huang, G.N., Acharya, A., Smith, C.L., et al., (2012). Heart repair by reprogramming non-myocytes with cardiac transcription factors. *Nature*, **485**, 599–604.
38. L. Wang, Z. Liu, C. Yin, H. Asfour, O. Chen, Y. Li, N. Bursac, J. Liu, L. Qian, Stoichiometry of Gata4, Mef2c, and Tbx5 influences the efficiency and quality of induced cardiac myocyte reprogramming, Circ. Res. (2015). https://www.ahajournals.org/doi/abs/10.1161/circresaha.116.305547 (accessed August 15, 2018).
39. Ueyama, T., Kasahara, H., Ishiwata, T., Nie, Q., Izumo, S., (2003). Myocardin expression is regulated by Nkx2.5, and its function is required for cardiomyogenesis. *Mol. Cell. Biol*, **23**, 9222–9232.
40. Creemers, E.E., Sutherland, L.B., McAnally, J., Richardson, J.A., Olson, E.N., (2006). Myocardin is a direct transcriptional target of Mef2, Tead and Foxo proteins during cardiovascular development. *Development*, **133**, 4245–4256.
41. Pagiatakis, C., Gordon, J.W., Ehyai, S., McDermott, J.C., (2012). A novel RhoA/ROCK-CPI-17-MEF2C signaling pathway regulates vascular smooth muscle cell gene expression. *J. Biol. Chem.*, **287**, 8361–8370.
42. Oki, S., Ohta, T., Shioi, G., Hatanaka, H., Ogasawara, O., Okuda, Y., Kawaji, H., Nakaki, R., et al., (2018). , ChIP-Atlas: a data-mining suite powered by full integration of public ChIP-seq data. *EMBO Rep*, **19**,https://doi.org/10.15252/embr.201846255.
[43] Lei, X., Kou, Y., Fu, Y., Rajashekar, N., Shi, H., Wu, F., Xu, J., Luo, Y., et al., (2018). The cancer mutation D83V induces an α-helix to β-strand conformation switch in MEF2B. *J. Mol. Biol.*, **430**, 1157–1172.
44. Han, A., Pan, F., Stroud, J.C., Youn, H.-D., Liu, J.O., Chen, L., (2003). Sequence-specific recruitment of transcriptional co-repressor Cabin1 by myocyte enhancer factor-2. *Nature*, **422**, 730–734.
45. Pradhan, L., Genis, C., Scone, P., Weinberg, E.O., Kasahara, H., Nam, H.-J., (2012). Crystal structure of the human NKX2.5 homeodomain in complex with DNA target. *Biochemistry*, **51**, 6312–6319.
[46] Gutierrez-Roelens, I., Sluysmans, T., Gewillig, M., Devriendt, K., Vikkula, M., (2002). Progressive AV-block and anomalous venous return among cardiac anomalies associated with two novel missense mutations in the CSX/NKX2–5 gene. *Hum. Mutat.*, **20**, 75–76.
47. Kasahara, H., Benson, D.W., (2004). Biochemical analyses of eight NKX2.5 homeodomain missense mutations causing atrioventricular block and cardiac anomalies. *Cardiovasc. Res*, **64**, 40–51.
48. Zakariyah, A.F., Rajgara, R.F., Veinot, J.P., Skerjanc, I.S., Burgon, P.G., (2017). Congenital heart defect causing mutation in Nkx2.5 displays in vivo functional deficit. *J. Mol. Cell. Cardiol*, **105**, 89–98.
[49] Zakariyah, A.F., Rajgara, R.F., Horner, E., Cattin, M.-E., Blais, A., Skerjanc, I.S., Burgon, P.G., (2018). In vitro modeling of congenital heart defects associated with an NKX2–5 mutation revealed a dysregulation in BMP/notch-mediated signaling. *Stem Cells*, **36**, 514–526.
50. E. Santelli, T.J. Richmond, Crystal structure of MEF2A core bound to DNA at 1.5 A resolution, J. Mol. Biol. 297 (2000) 437–449.
51. Hassler, M., Richmond, T.J., (2001). The B-box dominates SAP-1–SRF interactions in the structure of the ternary complex. *EMBO J.*, **20**, 3018–3028.
52. Mo, Y., Ho, W., Johnston, K., Marmorstein, R., (2001). Crystal structure of a ternary SAP-1/SRF/c-fos SRE DNA complex. *J. Mol. Biol.*, **314**, 495–506.
[53] Inga, A., Reamon-Buettner, S.M., Borlak, J., Resnick, M.A., (2005). Functional dissection of sequence-specific NKX2–5 DNA binding domain mutations associated with human heart septation defects using a yeast-based system. *Hum. Mol. Genet.*, **14**, 1965–1975.
[54] van Engelen, K., Mommersteeg, M.T.M., Baars, M.J.H., Lam, J., Ilgun, A., van Trotsenburg, A.S.P., Smets, A.M.J.B., Christoffels, V.M., et al., (2012). The ambiguous role of NKX2–5 mutations in thyroid Dysgenesis. *PLoS One*, **7**, e52685.
[55] Abou Hassan, O.K., Fahed, A.C., Batrawi, M., Arabi, M., Refaat, M.M., DePalma, S.R., Seidman, J.G., Seidman, C.E., et al., (2015). NKX2–5 mutations in an inbred consanguineous population: genetic and phenotypic diversity. *Sci. Rep.*, **5**, 8848.
[56] Kalayinia, S., Ghasemi, S., Mahdieh, N., (2019). A comprehensive in silico analysis, distribution and frequency of human Nkx2–5 mutations; a critical gene in congenital heart disease. *J. Cardiovasc. Thorac. Res.*, **11**, 287–299.
57. Kasahara, H., Izumo, S., (1999). Identification of the in vivo casein kinase II phosphorylation site within the homeodomain of the cardiac tisue-specifying homeobox gene product Csx/Nkx2.5. *Mol. Cell. Biol.*, **19**, 526–536.
[58] Hornbeck, P.V., Zhang, B., Murray, B., Kornhauser, J.M., Latham, V., Skrzypek, E., (2015). PhosphoSitePlus, 2014: mutations, PTMs and recalibrations. *Nucleic Acids Res.*, **43**, D512–D520.
59. Al Madhoun, A.S., Mehta, V., Li, G., Figeys, D., Wiper-Bergeron, N., Skerjanc, I.S., (2011). Skeletal myosin light chain kinase regulates skeletal myogenesis by phosphorylation of MEF2C. *EMBO J.*, **30**, 2477–2489.
60. He, J., Ye, J., Cai, Y., Riquelme, C., Liu, J.O., Liu, X., Han, A., Chen, L., (2011). Structure of p300 bound to MEF2 on DNA reveals a mechanism of enhanceosome assembly. *Nucleic Acids Res.*, **39**, 4464–4474.
[61] Cardoso, A.C., Pereira, A.H.M., Ambrosio, A.L.B., Consonni, S.R., Rocha de Oliveira, R., Bajgelman, M.C., Dias, S.M.G., Franchini, K.G., (2016). FAK forms a complex with MEF2 to couple biomechanical signaling to transcription in cardiomyocytes. *Structure*, **24**, 1301–1310.
62. Molkentin, J.D., Black, B.L., Martin, J.F., Olson, E.N., (1996). Mutational analysis of the DNA binding, dimerization, and transcriptional activation domains of MEF2C. *Mol. Cell. Biol.*, **16**, 2627–2636.
63. Molkentin, J.D., Black, B.L., Martin, J.F., Olson, E.N., (1995). Cooperative activation of muscle gene expression by MEF2 and myogenic bHLH proteins. *Cell*, **83**, 1125–1136.

[64] Ounzain, S., Pedrazzini, T., (2016). Super-enhancer lncs to cardiovascular development and disease. *Biochim. Biophys. Acta*, **1863**, 1953–1960.
65. Hnisz, D., Abraham, B.J., Lee, T.I., Lau, A., Saint-André, V., Sigova, A.A., Hoke, H.A., Young, R.A., (2013). Super-enhancers in the control of cell identity and disease. *Cell*, **155**, 934–947.
66. Wu, Y., Dey, R., Han, A., Jayathilaka, N., Philips, M., Ye, J., Chen, L., (2010). Structure of the MADS-box/MEF2 domain of MEF2A bound to DNA and its implication for myocardin recruitment. *J. Mol. Biol.*, **397**, 520–533.
[67] Collaborative Computational Project, (1994). Number 4, the CCP4 suite: programs for protein crystallography. *Acta Crystallogr. D Biol. Crystallogr.*, **50**, 760–763.
68. Battye, T.G.G., Kontogiannis, L., Johnson, O., Powell, H.R., Leslie, A.G.W., (2011). iMOSFLM: a new graphical interface for diffraction-image processing with MOSFLM. *Acta Crystallogr. D Biol. Crystallogr.*, **67**, 271–281.
69. Potterton, E., Briggs, P., Turkenburg, M., Dodson, E., (2003). A graphical user interface to the CCP4 program suite. *Acta Crystallogr. D Biol. Crystallogr.*, **59**, 1131–1137.
70. McCoy, A.J., Grosse-Kunstleve, R.W., Adams, P.D., Winn, M. D., Storoni, L.C., Read, R.J., (2007). Phaser crystallographic software. *J. Appl. Crystallogr.*, **40**, 658–674.
71. Emsley, P., Cowtan, K., (2004). Coot: model-building tools for molecular graphics. *Acta Crystallogr. D Biol. Crystallogr.*, **60**, 2126–2132.
[72] Adams, P.D., Afonine, P.V., Bunkóczi, G., Chen, V.B., Davis, I. W., Echols, N., Headd, J.J., Hung, L.-W., et al., (2010). PHENIX: a comprehensive python-based system for macromolecular structure solution. *Acta Crystallogr. D Biol. Crystallogr.*, **66**, 213–221.
73. Afonine, P.V., Grosse-Kunstleve, R.W., Echols, N., Headd, J. J., Moriarty, N.W., Mustyakimov, M., Terwilliger, T.C., Urzhumtsev, A., et al., (2012). Towards automated crystallographic structure refinement with phenix.refine. *Acta Crystallogr. D Biol. Crystallogr*, **68**, 352–367.
74. Joosten, R.P., Long, F., Murshudov, G.N., Perrakis, A., (2014). The PDB_REDO server for macromolecular structure model optimization. *IUCrJ.*, **1**, 213–220.
75. Joosten, R.P., Salzemann, J., Bloch, V., Stockinger, H., Berglund, A.-C., Blanchet, C., Bongcam-Rudloff, E., Combet, C., et al., (2009). PDB_REDO: automated re-refinement of X-ray structure models in the PDB. *J. Appl. Crystallogr.*, **42**, 376–384.
76. Hodel, A., Kim, S.-H., Brünger, A.T., (1992). Model bias in macromolecular crystal structures. *Acta Crystallogr. A.*, **48**, 851–858.
77. Terwilliger, T.C., Grosse-Kunstleve, R.W., Afonine, P.V., Moriarty, N.W., Adams, P.D., Read, R.J., Zwart, P.H., Hung, L.-W., (2008). Iterative-build OMIT maps: map improvement by iterative model building and refinement without model bias. *Acta Crystallogr. D Biol. Crystallogr.*, **64**, 515–524.
78. Afonine, P.V., Moriarty, N.W., Mustyakimov, M., Sobolev, O. V., Terwilliger, T.C., Turk, D., Urzhumtsev, A., Adams, P.D., (2015). FEM: feature-enhanced map. *Acta Crystallogr. D Biol. Crystallogr.*, **71**, 646–666.
79. Sievers, F., Wilm, A., Dineen, D., Gibson, T.J., Karplus, K., Li, W., Lopez, R., McWilliam, H., et al., (2011). Fast, scalable generation of high-quality protein multiple sequence alignments using Clustal Omega. *Mol. Syst. Biol.*, **7**, 539.
[80] Robert, X., Gouet, P., (2014). Deciphering key features in protein structures with the new ENDscript server. *Nucleic Acids Res.*, **42**, W320–W324.
81. Sagendorf, J.M., Markarian, N., Berman, H.M., Rohs, R., (2020). DNAproDB: an expanded database and web-based tool for structural analysis of DNA–protein complexes. *Nucleic Acids Res.*, **48**, D277–D287.
82. Thorvaldsdóttir, H., Robinson, J.T., Mesirov, J.P., (2013). Integrative Genomics Viewer (IGV): high-performance genomics data visualization and exploration. *Brief. Bioinform.*, **14**, 178–192.